

Keywords: MYO10; clinicopathological factor; breast cancer; invadopodia

Elevated expression of myosin X in tumours contributes to breast cancer aggressiveness and metastasis

R Cao¹, J Chen¹, X Zhang¹, Y Zhai¹, X Qing¹, W Xing², L Zhang², Y S Malik¹, H Yu¹ and X Zhu^{*1}

¹Laboratory of Molecular Epigenetics of Ministry of Education, Institute of Genetics and Cytology, Northeast Normal University, 5268 Renmin Street, Changchun, Jilin Province, China 130024 and ²Sino-Japanese Friendship Hospital, Jilin University, 126 Xiantai Street, Changchun, Jilin Province, China 130033

Background: Myosin X (MYO10) was recently reported to promote tumour invasion by transporting integrins to filopodial tips in breast cancer. However, the role of MYO10 in tumours remains poorly defined. Here, we report that MYO10 is required in invadopodia to mediate invasive growth and extracellular matrix degradation, which depends on the binding of MYO10's pleckstrin homology domain to PtdIns(3,4,5)P₃.

Methods: The expression of MYO10 and its associations with clinicopathological and biological factors were examined in breast cancer cells and breast cancer specimens ($n = 120$). Cell migration and invasion were investigated after the silencing of MYO10. The ability of cells to form invadopodia was studied using a fluorescein isothiocyanate-conjugated gelatin degradation assay. A mouse model was established to study tumour invasive growth and metastasis *in vivo*.

Results: Elevated MYO10 levels were correlated with oestrogen receptor status, progesterone receptor status, poor differentiation, and lymph node metastasis. Silencing MYO10 reduced cell migration and invasion. Invadopodia were responsible for MYO10's role in promoting invasion. Furthermore, decreased invasive growth and lung metastasis were observed in the MYO10-silenced nude mouse model.

Conclusions: Our findings suggest that elevated MYO10 expression increases the aggressiveness of breast cancer; this effect is dependent on the involvement of MYO10 in invadopodial formation.

Breast cancer is the most common malignancy and the second leading cause of cancer death among females (DeSantis *et al*, 2011). However, the molecular mechanism of the growth and development of breast cancer remains unclear. Clinically, the tumour differentiation grade, that is, the histological grade based on tumour cell mitosis, cell differentiation, and nuclear pleomorphism, is an indicator of disease aggressiveness and an independent prognostic biomarker (Rakha *et al*, 2010). Currently, three important receptors, that is, oestrogen receptor (ER), progesterone receptor (PR), and human epidermal growth factor receptor 2 (Her2), are established biomarkers in common clinical use as disease status indicators and therapeutic targets (Jordan and Morrow, 1999; Gianni *et al*, 2010; Lv *et al*, 2013).

Breast cancer metastasis reflects the extent of disease aggressiveness and progression (Minn *et al*, 2005). Typically, cancer metastasis is a complex process involving tumour cells initiating actin-rich membrane protrusions to invade surrounding tissues and intravasate through the endothelium to enter the systemic circulation. The protrusive structures formed by migrating cells are termed filopodia, lamellipodia, and invadopodia/podosomes, depending on their morphological, structural, and functional characteristics (Yamaguchi and Condeelis, 2007). Invadopodia are protrusions from invading cells; these actin-based protrusions regulate actin polymerisation and degrade the extracellular matrix (ECM) via the localisation of proteases (Chen, 1989). The ability to mediate focal ECM degradation

*Correspondence: Dr X Zhu; E-mail: zhuxj720@nenu.edu.cn

Received 21 January 2014; revised 1 May 2014; accepted 9 May 2014; published online 12 June 2014

© 2014 Cancer Research UK. All rights reserved 0007–0920/14

suggests a critical role for invadopodia in tumour metastasis (Eckert *et al*, 2011).

Myosin X (MYO10), a molecular motor located at the tips of filopodia, is essential for many cell processes, including wound healing (Wood *et al*, 2002), filopodial formation (Berg and Cheney, 2002), angiogenesis (Gerhardt *et al*, 2003), the regulation of growth cone formation and turning (Yu *et al*, 2012), and invadopodia formation (Schoumacher *et al*, 2010). MYO10 has the ability to move along actin filaments (Sousa and Cheney, 2005). The FERM domain of MYO10 is reportedly a binding domain for specific cargo molecules, including integrins (Zhang *et al*, 2004), Mena/VASP (Tokuo and Ikebe, 2004), DCC (Zhu *et al*, 2007), and VE-cadherin (Almagro *et al*, 2010). Recently, MYO10 was reported to mediate breast tumour cell invasion by transporting integrins to the filopodial tip (Arjonen *et al*, 2014). However, the mechanism by which MYO10 controls tumour invasive growth and metastasis is poorly understood.

In this study, we examined the correlation between MYO10 and aggressiveness and metastasis in human clinical breast cancer specimens. An analysis of clinicopathological and biological factors revealed associations between *MYO10* and ER status, PR status, differentiation grade, and lymph node metastasis. MYO10 exerted

a direct effect on invadopodia to promote tumour invasive growth and lung metastasis in a nude mouse model. These data suggest that MYO10 is a novel independent prognostic biomarker for breast cancer.

MATERIALS AND METHODS

Antibodies. The antibodies used in this study are listed in the Supplementary Materials and Methods.

Clinical specimens. This study was approved by the Regional Ethical Review Board of Jilin University and Northeast Normal University. Informed consent was obtained from all of the patients recruited for this study. The specimens were obtained from consecutive patients who underwent surgery without any neo-adjuvant therapy between February 2012 and March 2013. Fresh tumour tissues, adjacent nonmalignant tissues, and the corresponding normal tissues were resected and immediately frozen in liquid nitrogen (*n* = 120, Supplementary Table S1). For the western blots shown in Figure 1A and B, samples were selected randomly; the sequence numbers correspond to the patient numbers in

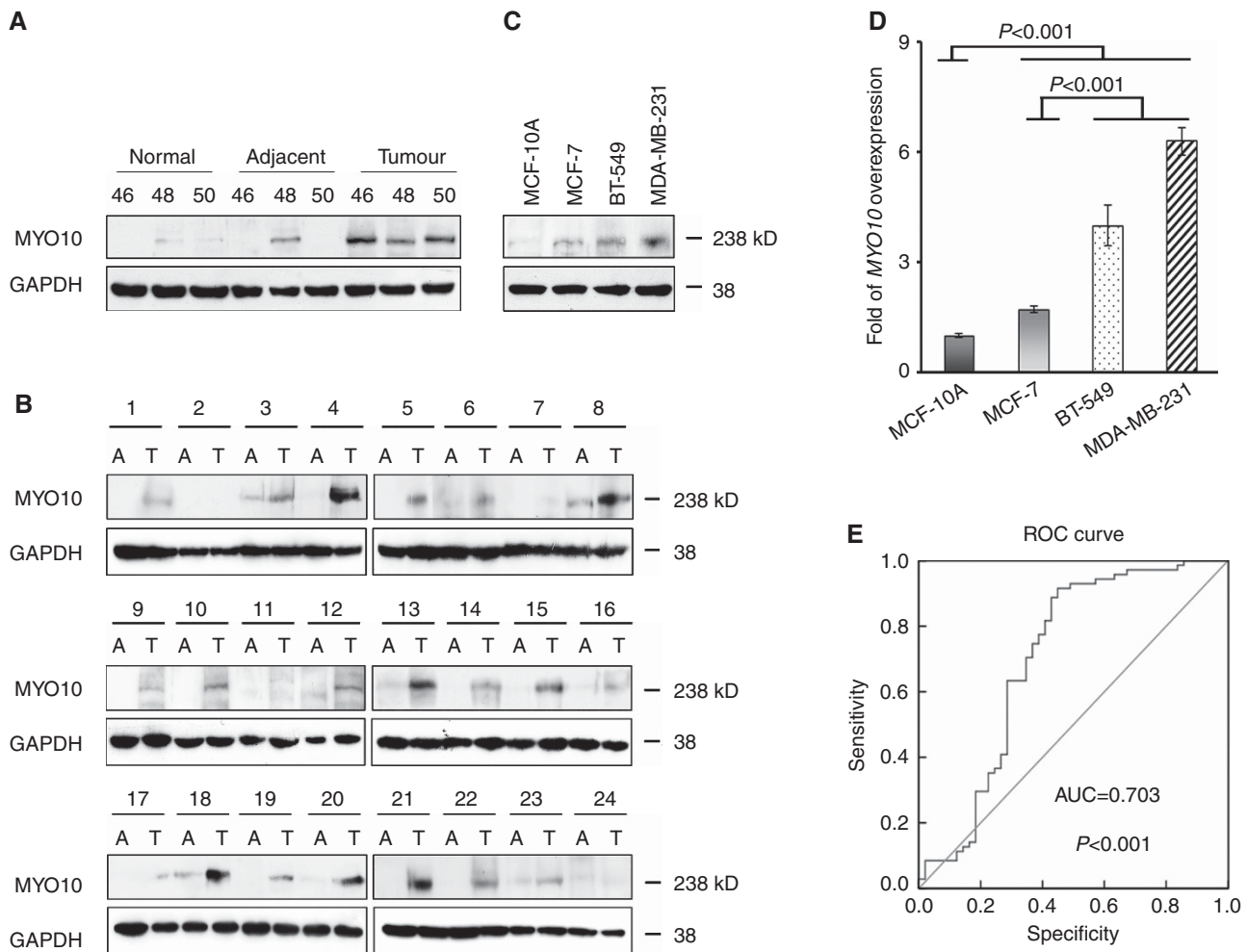


Figure 1. Elevated expression of MYO10 in breast cancer tissues and cultured cells. (A) Representative western blots of MYO10 in normal epithelial tissues, adjacent nonmalignant tissues, and breast cancer tissues from three patients (nos. 46, 48, and 50). GAPDH was used as a loading control. (B) Western blots of MYO10 in tumour tissues (T) and adjacent nonmalignant tissues (A) from an additional 24 patients (nos. 1–24). (C) Representative western blots of MYO10 expression in MCF-10A, MCF-7, BT-549, and MDA-MB-231 cells. (D) Relative expression levels of MYO10 in breast cancer cells using quantitative PCR. The expression of MYO10 in MCF-10A was normalised to 1. (E) Receiver operating characteristic (ROC) curves for MYO10. The area under the ROC curve (AUC) was 0.703. The results shown are representative of three independent experiments. The bars and error bars represent the means ± s.e., and the *P*-value was calculated using an independent *t*-test.

Supplementary Table S1. Immunohistochemical staining results were obtained from patient records, and all of the sections were examined by two independent pathologists. Based on the immunohistochemical staining results for ER, PR, Her2, and Ki-67, the patients were classified into four clinicopathological subtypes: luminal A (ER+, PR+, Her2-, and Ki-67 < 14%); luminal B (ER+, PR+, Her2-, and Ki-67 ≥ 14%; or ER+, PR+, and Her2+); Her2+ (ER-, PR-, and Her2+); and triple-negative breast cancer (TNBC; ER-, PR-, and Her2-) (Park *et al.*, 2012).

Cell lines and cell culture. The cell lines used in this study and the cell culture methods are detailed in the Supplementary Materials and Methods.

Cell/tissue lysis and immunoblotting. Standard procedures for cell/tissue lysis and immunoblotting are described in the Supplementary Materials and Methods.

Quantitative PCR analysis. The quantitative PCR protocol and primers are described in the Supplementary Materials and Methods.

Lentiviral packaging and transfection. A description of the lentiviral packaging and transfection procedure is detailed in the Supplementary Materials and Methods.

Transwell migration and invasion assay. Transwell migration and invasion experiments were performed as described in the Supplementary Materials and Methods.

Cell proliferation assay. Cell growth rates were assessed via the MTT assay, as described in the Supplementary Materials and Methods.

Expression profiling. A description of the expression profiling procedure is detailed in the Supplementary Materials and Methods.

Microarray data processing. The microarray data processing protocol is described in the Supplementary Materials and Methods.

Zymography assay. Zymography experiments were performed as described in the Supplementary Materials and Methods.

Gelatin degradation assay. Fluorescein isothiocyanate-conjugated gelatin (FITC-gelatin) matrix (100 μl, 0.2% gelatin in PBS, EPC no. GF759) was added to each coverslip, incubated overnight, and fixed with 0.5% glutaraldehyde for 50 min on ice. The residual reactive groups in the gelatin matrix were quenched with 5 mg ml⁻¹ sodium borohydride for 3 min. Coverslips were incubated in DMEM with 10% FBS at 37 °C for 4 h before use.

Cells were plated onto coverslips coated with FITC-gelatin, incubated at 37 °C for 12 h, and processed for immunofluorescence. Matrix degraded by invadopodia appeared as 'holes' in the bright fluorescent gelatin. To quantitate cells with invadopodia or the ECM degradation by invadopodia, 10 randomly selected fields were visualised using a × 60 objective for each calculation. ImageJ software (National Institutes of Health, Bethesda, MD, USA) was used to determine the number of cells with invadopodia with respect to the total cell number and the degraded area relative to the cell area. Each experiment was performed in triplicate and was repeated at least three times. The MYO10 DN and KK1225/6AA plasmids have been described previously (Yu *et al.*, 2012). The PI3K inhibitor LY294002 (Sigma Aldrich, St Louis, MO, USA) was used at a final concentration of 30 μM.

Immunofluorescence staining. The immunofluorescence staining experiments were performed as described in the Supplementary Materials and Methods.

Mouse xenograft models. All of the experimental protocols and procedures involving mice, including housing and care, were approved by the Institutional Animal Care and Use Committee of

Northeast Normal University according to the guidelines of the Committee of the National Cancer Research Institute (Workman *et al.*, 2010). For the tumour growth model, 1.5×10^6 cells in 100 μl of PBS were seeded into the left mammary fat pads of 6-week-old female BALB/c nude mice on day 0. Tumour size was measured using calipers every other day, and tumour volume was calculated using the formula $(W^2 \times L)/2$, where W and L represent the larger and smaller tumour diameters, respectively. The mice were killed on day 42. The tissues were embedded in paraffin or OCT compound (Tissue-Tek, Sakura Finetek Co., Ltd., Tokyo, Japan), sectioned, and stained with haematoxylin and eosin (HE) or used for immunofluorescence staining.

For the lung carcinoma metastasis model, 1.5×10^6 cells in 100 μl of PBS were injected into the tail vein. After 3 weeks, the lungs were harvested and examined for EGFP-positive cells. Tissues were embedded in paraffin or OCT compound, sectioned, and stained with HE or examined directly for EGFP-positive foci.

Statistical analysis. SPSS17.0 (Chicago, IL, USA) was used to perform the statistical analyses. The data are presented as the means ± the standard error if three or more independent repeats were performed. A one-way analysis of variance was used for comparisons of patient ages, tumour sizes, and breast cancer subtypes. Independent *t*-tests were used for comparisons of tumour grades; ER, PR, and Her2 status; and other data between the two groups. Receiver operating characteristic (ROC) curves were used to assess whether MYO10 is a predictive marker of lymph node metastasis (Zou *et al.*, 2007). Univariate and multivariate logistic regressions (backward) were used to analyse the associations between elevated MYO10 expression and tumour differentiation grade and lymph node metastasis in clinical specimens. $P < 0.05$ was considered significant, and $P < 0.001$ was considered extremely significant.

RESULTS

Elevated expression of MYO10 in breast cancer specimens and cell lines. The expression of MYO10 was first evaluated in clinical specimens from breast cancer patients. Western blots revealed that MYO10 expression was almost undetectable in normal mammary epithelial tissues, was abundant in breast carcinoma tissues, and was detected (at a low level) in some of the adjacent nonmalignant tissues (Figure 1A; Supplementary Figure S1A). To further confirm the elevated expression of MYO10 protein in tumours, paired adjacent and tumour tissues from an additional 24 patients were collected and analysed. The MYO10 expression in these tumours was consistently and dramatically increased in 21 of the 24 patients (87%) (Figure 1B; Supplementary Figure S1B).

The MYO10 expression profile was then characterised in the following four types of cell lines: MCF-10A human mammary epithelial cells, which are nontumorigenic (Yang *et al.*, 1997); MCF-7 human breast carcinoma cells, which are tumorigenic but nonmetastatic (Fang *et al.*, 2010); and BT-549 and MDA-MB-231 cells, which are invasive and metastatic *in vivo* and *in vitro* (Gilles *et al.*, 1998). The results revealed that the expression of the MYO10 protein was low in the MCF-10A cells, slightly higher in the MCF-7 cells, and significantly higher in the highly invasive BT-549 and MDA-MB-231 cells (Figure 1C; Supplementary Figure S1C). In agreement with the protein analysis, significantly more MYO10 mRNA was observed in the BT-549 and MDA-MB-231 cells than in the MCF-10A and MCF-7 cells (Figure 1D, $P < 0.001$). Our findings confirmed the elevated expression of MYO10 in breast cancer tissues *in vivo* and in cultured cells *in vitro*.

MYO10 was associated with aggressive breast cancer subtypes. To clarify the association between MYO10 and clinical aggressiveness in breast cancer patients, the MYO10 mRNA profile was then

examined in breast cancer specimens from 120 patients. Of these, 110 patients (91.67%) exhibited elevated expression of *MYO10* in the tumour tissues compared with the adjacent nonmalignant tissues (*MYO10* in adjacent tissue was normalised to 1, Supplementary Table S1). ER and PR are two molecular prognostic markers used in breast cancer patients. Elevated *MYO10* expression was observed in the ER- tumours relative to the ER+ tumours and in the PR- tumours relative to the PR+ tumours (Table 1, $P < 0.001$). However, there was no significant difference in *MYO10* expression between the patients with Her2+ and Her2- tumours (Table 1).

Breast cancer is often classified into four molecular subtypes, according to the status of ER, PR, Her2, and Ki-67, to guide clinical treatment decision making and follow-up strategies (Park *et al*, 2012). Table 1 demonstrates that among the 120 patients, the 31 cases of the Her2 subtype (25.83%) exhibited elevated *MYO10* expression ($P < 0.001$) compared with the luminal A and B subtypes (Table 1). In the 20 (20/120, 16.67%) TNBC patients, *MYO10* expression was elevated 7-fold

compared with the adjacent nonmalignant tissues and was significantly higher than in the luminal A/B and Her2 patients (Table 1, $P < 0.001$). These findings confirmed that *MYO10* expression was associated with aggressive breast cancer subtypes and may be a prognostic factor in treatment decision making.

***MYO10* was associated with breast cancer aggressiveness and metastasis in clinical patients.** Tumour differentiation grade and the presence (N+) or absence (N-) of regional lymph node spread (N stage) are well-established independent factors for predicting disease aggressiveness and patient survival (Bloom and Richardson, 1957). Of the 120 breast cancer patients in this study, 45 (37.5%) had grade 3 disease. *MYO10* expression in these patients was dramatically elevated compared with those patients with grade 1/2 disease (Table 1, $P < 0.001$). Similarly, the patients with lymph node metastases (71/120, 59.17%) exhibited elevated *MYO10* expression compared with the nonmetastatic patients (Table 1, $P = 0.002$). To further characterise the role of *MYO10* expression

Table 1. *MYO10* expression correlated with clinicopathological and biological factors in 120 breast cancer specimens^a

Factor	Variable	n (%)	Fold of <i>MYO10</i> expression (means \pm s.e.)	P-value
Age				0.198 ^b
	≤ 45	48 (40.00)	3.637 \pm 0.338	
	45–60	56 (46.67)	4.198 \pm 0.288	
	> 60	16 (13.33)	4.759 \pm 0.678	
Size (mm)				0.069 ^b
	<20 (stage T1)	44 (36.67)	3.663 \pm 0.356	
	20–50 (stage T2)	63 (52.50)	4.050 \pm 0.285	
	≥ 50 (stage T3)	13 (10.83)	5.349 \pm 0.580	
ER				0.000 ^c
	Positive	70 (58.33)	2.934 \pm 0.206	
	Negative	50 (41.67)	5.608 \pm 0.304	
PR				0.000 ^c
	Positive	68 (56.67)	2.841 \pm 0.203	
	Negative	52 (43.33)	5.628 \pm 0.290	
Her2				0.521 ^c
	Positive	45 (37.50)	3.872 \pm 0.262	
	Negative	75 (62.50)	4.154 \pm 0.300	
Luminal A vs B				0.227 ^c
	A (ER+, PR+, Her2-, Ki-67 <14%)	22 (18.33)	3.238 \pm 0.400	
	B (ER+, PR+, Her2-, Ki-67 $\geq 14\%$; or ER+, PR+, Her2+)	47 (39.17)	2.708 \pm 0.232	
Her2 subtype ^d				0.000 ^c
	ER-, PR-, Her2+	31 (25.83)	4.523 \pm 0.291	
Triple negative (ER-, PR-, Her2-)				0.000 ^c
	Yes	20 (16.67)	7.354 \pm 0.350	
	No	100 (83.33)	3.387 \pm 0.183	
Tumour differentiation grade				0.000 ^c
	Grade 1/2	75 (62.50)	2.883 \pm 0.200	
	Grade 3	45 (37.50)	5.990 \pm 0.271	
Lymph node metastasis				0.002 ^c
	No (N-)	49 (40.83)	3.255 \pm 0.361	
	Yes (N+)	71 (59.17)	4.596 \pm 0.238	

^aFold of *MYO10* expression (*GAPDH* as control) in breast cancer tissue over adjacent nonmalignant tissue from the same specimen. Triple repeated per specimen.

^bOne-way ANOVA.

^cIndependent t-test.

^dCompared with luminal A and B.

in lymph node metastasis, we calculated ROC curves (Zou *et al*, 2007). The results revealed that the area under the curve of *MYO10* in the patients with lymph node metastasis was 0.703 ($P < 0.001$), with a sensitivity of 0.915 and a specificity of 0.551 (Figure 1E), indicating that *MYO10* may be an independent factor in predicting lymph node metastasis.

Breast tumour size is a key factor in determining T stages (T1 < 20 mm, 20 mm ≤ T2 < 50 mm, and T3 ≥ 50 mm), according to the American Joint Committee on Cancer (AJCC) Cancer Staging Manual, 6th and 7th editions. We observed a positive correlation between *MYO10* expression and tumour size (Table 1). The *MYO10* expression in stage T3 tumours was significantly higher than in stage T1 tumours (Table 1, $P = 0.031$). None of the tissues assessed in this study were from patients with distant metastases or stage T4 disease, most likely because such patients would not have been selected as candidates for definitive surgical treatment.

We performed both univariate and multivariate analyses using binary logistic regression (backward) to characterise the associations and interactions in breast cancer aggressiveness and metastasis of all of the above individual clinicopathological factors, biological makers, and molecular markers, including *MYO10* expression, patient age at diagnosis, tumour size, T and N stages, menopause status, and ER, PR, Her2, p53, and Ki-67 expression status. The results of both the univariate and multivariate analyses

revealed significant positive correlations between elevated *MYO10* expression and tumour differentiation grade (Table 2, upper part; odds ratio (OR) = 2.480 in the univariate and 3.964 in the multivariate analysis, $P < 0.001$) and lymph node metastasis (Table 2, lower part; (OR) = 1.324, $P = 0.003$ in the univariate and (OR) = 1.286, $P = 0.009$ in the multivariate analysis). Thus, *MYO10* is a potential molecular marker of clinical breast cancer progression.

Silencing *MYO10* reduced cell migration and invasiveness *in vitro*. Our findings that elevated *MYO10* expression in breast cancer patients was associated with lymph node metastasis and with the subtypes with poor outcomes led us to hypothesise that the mechanism underlying these effects of *MYO10* might be associated with enhanced cell motility. Therefore, EGFP-tagged silencing vectors specifically targeting human *MYO10* mRNA (*MYO10* shRNA¹⁹⁷¹, *MYO10* shRNA³²⁹⁹, and scrambled shRNA as control) were constructed. Silencing efficiency was confirmed by western blots (Figure 2A and B) in TNBC MDA-MB-231 cells. A transwell assay revealed that the number of cells successfully migrating through the uncoated membranes was 53.1% lower in *MYO10* shRNA¹⁹⁷¹ cells and 44.5% lower in *MYO10* shRNA³²⁹⁹ cells than in scrambled shRNA cells ($n = 30$ per sample, $P < 0.001$, Figure 2C). Silencing *MYO10* also led to reductions of 50.6% and

Table 2. *MYO10* expression associated with breast cancer aggressiveness (tumour differentiation grade) and lymph node metastasis^a

	Univariate		Multivariate			
	Odds ratio	P-value	95% Confidence level			
			Odds ratio	Lower	Upper	P-value
Tumour differentiation grade 1/2 (moderately differentiated, reference) vs grade 3 (poorly differentiated or undifferentiated)						
Ratio of children and pregnancies (%)	2.129	0.362				
Tumour volume (cc)	1.018	0.104				
Stage T1 (reference)	1.000	0.129				
Stage T2	1.769	0.154				
Stage T3	3.833	0.084				
Positive lymph node metastasis (negative as reference)	2.678	0.016				
p53	1.014	0.011				
Progesterone receptor positive (negative as reference)	0.102	0.000				
Age	1.028	0.125	0.917	0.839	1.002	0.056
Non-menopause (menopause as reference)	2.737	0.010	7.156	1.014	50.478	0.048
Oestrogen receptor positive (negative as reference)	0.153	0.000	4.826	0.951	24.486	0.057
Her2 positive (negative as reference)	2.519	0.018	20.865	3.951	110.174	0.000
Ki-67	1.042	0.000	1.038	1.006	1.071	0.020
<i>MYO10</i> in tumour tissue (adjacent tissue as reference)	2.480	0.000	3.964	2.251	6.979	0.000
Negative lymph node metastasis (N0, reference) vs positive (N+)						
Age	1.008	0.625				
Tumour volume (cc)	1.057	0.020				
Tumour differentiation grade 3 (grade 1/2 as reference)	2.678	0.016				
Non-menopause (menopause as reference)	1.296	0.493				
Oestrogen receptor positive (negative as reference)	0.528	0.098				
Progesterone receptor positive (negative as reference)	0.471	0.051				
p53	1.007	0.207				
Ki-67	1.011	0.240				
Stage T1 (reference)	1.000	0.064	1.000			0.151
Stage T2	2.581	0.019	2.338	0.994	5.499	0.052
Stage T3	> 1000	0.999	> 1000	0.000	> 1000	0.999
Ratio of children and pregnancies	3.532	0.119	4.932	0.800	30.413	0.086
Her2 positive (negative as reference)	2.678	0.016	2.397	0.994	5.776	0.051
<i>MYO10</i> in tumour tissue (adjacent tissue as reference)	1.324	0.003	1.286	1.065	1.553	0.009

^aBinary logistic regression (backward) in 120 breast cancer specimens. Triple repeated per specimen.

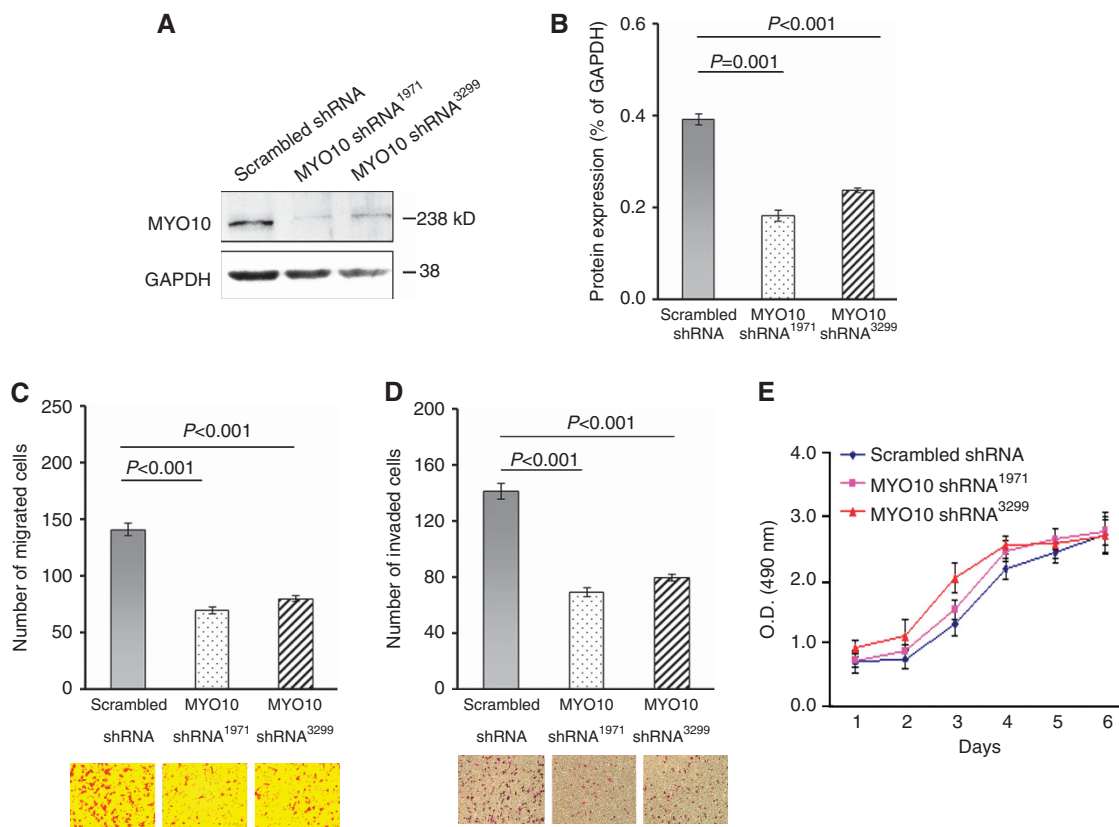


Figure 2. Silencing MYO10 reduces cell migration and invasion *in vitro*. (A) Western blots of MYO10 in MDA-MB-231 cells transfected with scrambled shRNA (control), MYO10 shRNA¹⁹⁷¹, or MYO10 shRNA³²⁹⁹; GAPDH served as a loading control. (B) A relative densitometry analysis of the protein expression (normalised to GAPDH) in Figure 2A. (C) Cell migration assay of MDA-MB-231 cells transfected with MYO10 shRNA¹⁹⁷¹, MYO10 shRNA³²⁹⁹, or scrambled shRNA as a control ($n = 30$ per sample). (D) Cell invasion assay of MDA-MB-231 cells transfected with scrambled shRNA, MYO10 shRNA¹⁹⁷¹, or MYO10 shRNA³²⁹⁹ ($n = 24$ per sample). (E) Proliferation assays of cells transfected with scrambled shRNA, MYO10 shRNA¹⁹⁷¹, or MYO10 shRNA³²⁹⁹. The results shown are representative of three independent experiments. The bars and error bars represent the means \pm s.e., and the P -value was calculated using an independent t -test.

43.2% in the numbers of MYO10 shRNA¹⁹⁷¹ and MYO10 shRNA³²⁹⁹ cells invading through Matrigel-coated membranes, respectively ($n = 24$ per sample, $P < 0.001$, Figure 2D). However, the MTT assay did not reveal a significant inhibition of cell proliferation as a result of MYO10 silencing (Figure 2E). Taken together, the *in vitro* findings indicated that MYO10 silencing significantly affected directional migration and invasion, critical cellular data for elucidating the association between MYO10 and breast cancer aggressiveness.

Silencing MYO10 downregulated the expression of genes involved in invadopodium formation. Silencing MYO10 inhibited migration and invasion behaviours *in vitro*. To assess whether functionally related genes were downregulated upon MYO10 silencing, both sample groups (scrambled shRNA and MYO10 shRNA¹⁹⁷¹) were assayed using the Affymetrix Human Genome U133 plus 2.0 array ($n = 3$, Supplementary Table S2). Based on functional annotations and previous publications, the microarray expression data indicated that several genes involved in cell movement were downregulated by silencing MYO10 (Figure 3A). Furthermore, several downregulated genes closely associated with invadopodial formation (Figure 3A, underlined), including *CAPN2* (Cortesio *et al*, 2008), *MMP14* (Akanuma *et al*, 2014), *CD44* (Gimona *et al*, 2008), *RAC1* (Harper *et al*, 2010), and *CAV1* (Yamaguchi *et al*, 2009), were validated using quantitative PCR (Figure 3B). Key invadopodium-related proteins were analysed by western blots. We found that one invadopodium marker, cortactin (phospho Y421), was

significantly reduced by MYO10 silencing (Figure 3C and D, arrowhead). Remarkably, MYO10 shRNA¹⁹⁷¹ reduced the expression of matrix metalloprotease 14 (MMP-14) (Figure 3C and D, arrowhead). The amount of active MMP-9 secreted into the medium was also reduced, as shown by the zymography assay (Figure 3C and D, arrowhead). These results demonstrated that invadopodium formation was a possible explanation for the correlation between MYO10 expression and tumour aggressiveness.

Invadopodia were responsible for MYO10-promoted invasive growth. Invadopodia are believed to induce local invasion and metastasis in breast cancer cells (Eckert *et al*, 2011). The results of the FITC-gelatin degradation assay revealed that only BT-549 and MDA-MB-231 cells, which expressed abundant MYO10, formed invadopodia and degraded ECM, whereas MCF-7 and MCF-10A cells, both of which expressed minimal MYO10, did not (Figure 4A–C). Silencing MYO10 abolished the MYO10-associated promotion of invadopodium formation and ECM degradation (Figure 4D). The number of cells with invadopodia was reduced by silencing MYO10 in both MDA-MB-231 and BT-549 cells ($P < 0.001$, Figure 4E). Moreover, ECM degradation was also reduced in both cell lines ($P < 0.001$, Figure 4F).

It has been reported that the binding of MYO10 to PtdIns(3,4,5)P₃ is critical for the localisation of MYO10 and filopodium formation (Plantard *et al*, 2010). Therefore, we examined whether the promotion of invadopodium formation and ECM degradation by MYO10 exhibited a similar dependence

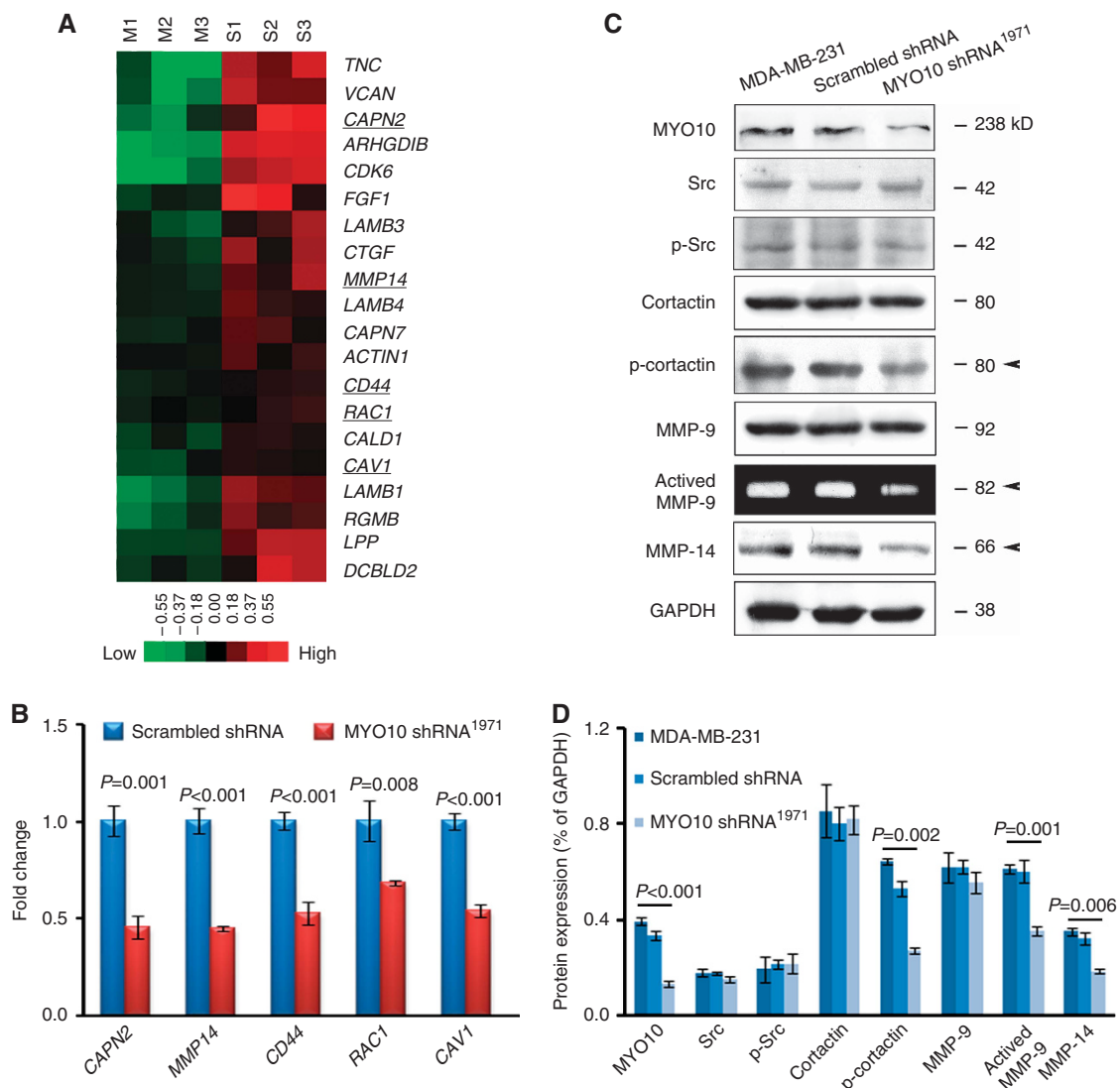


Figure 3. Silencing MYO10 downregulates genes involved in invadopodium formation. **(A)** The heatmap depicts the genes involved in cell movement activity and invadopodium formation (underlined) that were downregulated by MYO10 shRNA¹⁹⁷¹. Each row represents a transcript; each column represents a sample (green, low expression; M, MYO10 shRNA¹⁹⁷¹; S, scrambled shRNA). **(B)** The downregulation of these genes was validated using quantitative PCR. Gene expression in cells transfected with scrambled shRNA was normalised to 1. **(C)** The expression of key invadopodium-related proteins, including Src, p-Src, Cortactin, p-cortactin, MMP-9, and MMP-14, was analysed using western blots. The amount of active MMP-9 was analysed using a zymography assay. Arrows indicate reduced expression in cells transfected with MYO10 shRNA¹⁹⁷¹. **(D)** Relative densitometry analysis of the protein expression (normalised to GAPDH) in Figure 3C. The results are representative of three independent experiments. The bars and error bars represent the means ± s.e., and the P-value was calculated using an independent t-test.

on PtdIns(3,4,5)P3. MDA-MB-231 cells were transfected with a dominant-negative MYO10 plasmid (MYO10 DN) containing three pleckstrin homology (PH) domains, a MyTH4 domain, and a FERM domain in the C-terminal region. As shown in Figure 4G–I, the MYO10 DN-transfected cells exhibited impaired invadopodium formation and ECM degradation. Interestingly, similar phenotypes were obtained by incubating MDA-MB-231 cells with a phosphoinositide 3-kinase inhibitor, LY294002 (Figure 4G–I). However, cells transfected with KK1225/6AA, a plasmid bearing point mutations in the second PH domain of MYO10 DN, a key site for the binding of MYO10 to PtdIns(3,4,5)P3, recovered the ability to form invadopodia and degrade the ECM (Figure 4G–I). These results indicated that the elevated expression of MYO10 in invasive breast cancer cells enhanced invadopodium formation and ECM degradation, and this effect was dependent on binding between the second PH domain of MYO10 and PtdIns(3,4,5)P3.

Silencing MYO10 inhibited tumour growth and lung metastasis *in vivo*. To validate the above finding *in vivo*, tumour cells were injected into mouse mammary fat pads to assess invasive growth (Figure 5A). Thirty-two days after the injection, a significant difference in tumour size was observed between the groups injected with scrambled shRNA and MYO10 shRNA¹⁹⁷¹ (1102.63 ± 163.81 mm³ vs 576.05 ± 134.90 mm³, P = 0.038, Figure 5B). On day 42, the mice were sacrificed; the tumours were removed (Figure 5C) and examined using EGFP imaging (Figure 5D). The expression of MYO10 shRNA¹⁹⁷¹ decreased the tumour weight (scrambled shRNA 3.65 ± 0.41 g vs MYO10 shRNA¹⁹⁷¹ 1.53 ± 0.29 g, Figure 5E, P = 0.003) and restored tumour encapsulation, whereas tumours composed of scrambled shRNA cells invaded the surrounding stroma and adjacent adipose tissue (Figure 5F, HE staining). More importantly, silencing MYO10 reduced the number of cortactin-positive puncta, a marker of invadopodia, in primary tumour tissue sections (2.30 ± 0.17 per cell vs 0.48 ± 0.12 per cell, P < 0.001, Figure 5G and H).

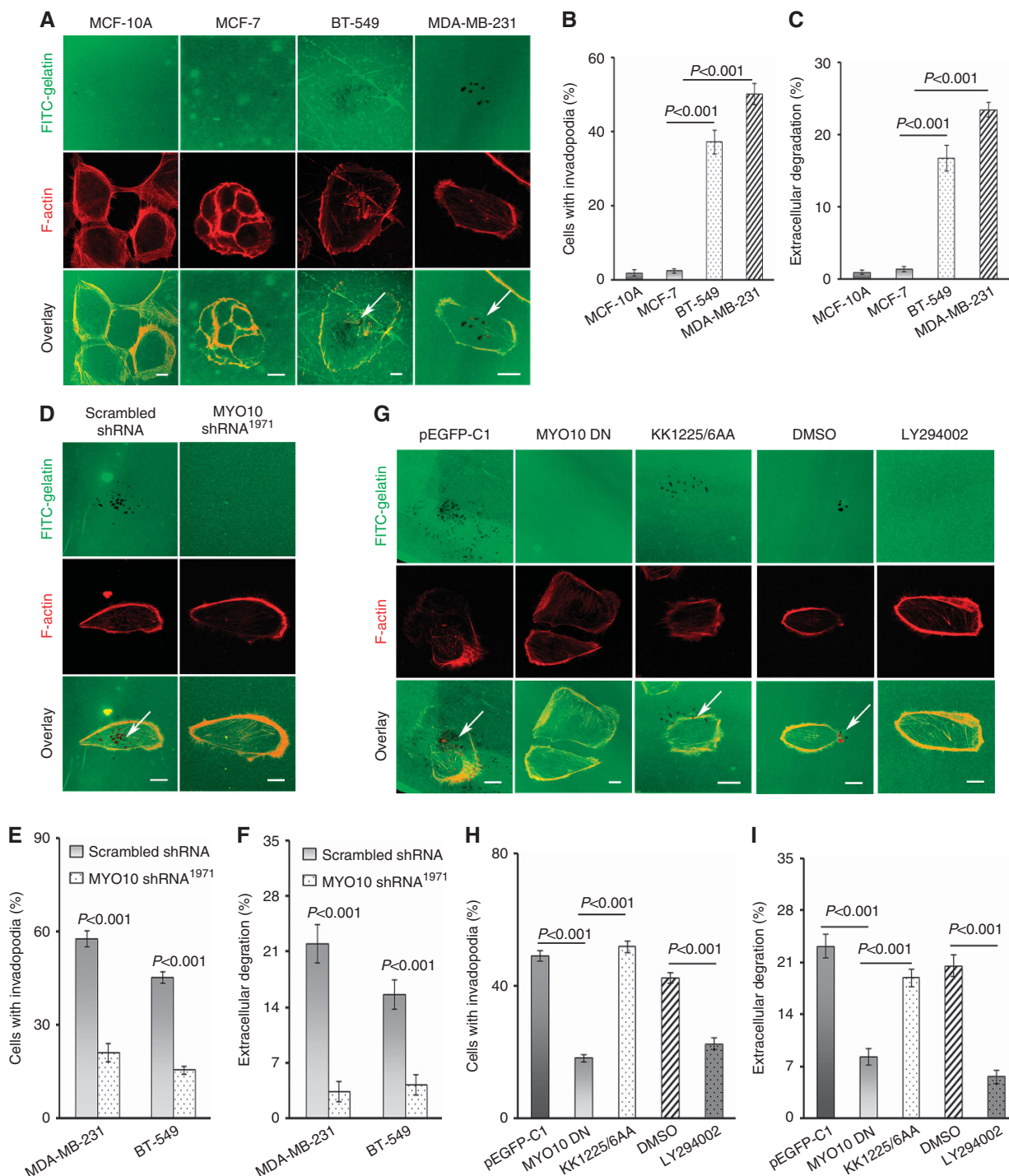


Figure 4. MYO10 functions in invadopodium formation and ECM degradation through binding with PtdIns(3,4,5)P3. **(A)** Invadopodium formation and ECM degradation in cultured cells. MCF-10A, MCF-7, BT-549, and MDA-MB-231 cells were plated on FITC-gelatin for 12 h, and F-actin (red) and the nuclei (data not shown) were stained to show invadopodium formation. Areas of gelatin degradation appear as dark spots in the fluorescent background beneath the cells (arrows). **(B)** Quantification of cells forming invadopodia using ImageJ software ($n = 100$ cells per sample). **(C)** Quantification of FITC-gelatin degradation using ImageJ software ($n = 100$ cells per sample). **(D)** Invadopodium formation and ECM degradation were inhibited by MYO10 shRNA. Cells expressing scrambled shRNA and MYO10 shRNA¹⁹⁷¹ were plated on FITC-gelatin for 12 h and were stained for F-actin (red). **(E)** Quantification of cells with invadopodia. Silencing MYO10 reduced invadopodium formation in MDA-MB-231 cells ($n = 67$ cells per sample, $P < 0.001$) and in BT-549 cells ($n = 40$ cells per sample, $P < 0.001$). **(F)** Quantification of FITC-gelatin degradation. Silencing MYO10 reduced ECM degradation in MDA-MB-231 cells ($n = 67$ cells per sample, $P < 0.001$) and in BT-549 cells ($n = 40$ cells per sample, $P < 0.001$). **(G)** MYO10 functions in invadopodium formation and ECM degradation by binding to PtdIns(3,4,5)P3. MDA-MB-231 cells were transfected with pEGFP-MYO10 DN (pEGFP-C1 as a control) or KK1225/6AA or were incubated with a PtdIns(3,4,5)P3 inhibitor (30 μ M LY294002, DMSO as a control) and were plated on FITC-gelatin for 12 h and stained for F-actin (red). **(H)** Quantification of cells with invadopodia among cells transfected with plasmids or incubated with LY294002 or DMSO ($n = 100$ cells per sample). **(I)** Quantification of FITC-gelatin degradation from the cells transfected with plasmids or incubated with LY294002 or DMSO ($n = 100$ cells per sample). The data are presented as the means \pm s.e. based on three independent repeats. The P -value was calculated using an independent t -test. Bars, 10 μ m.

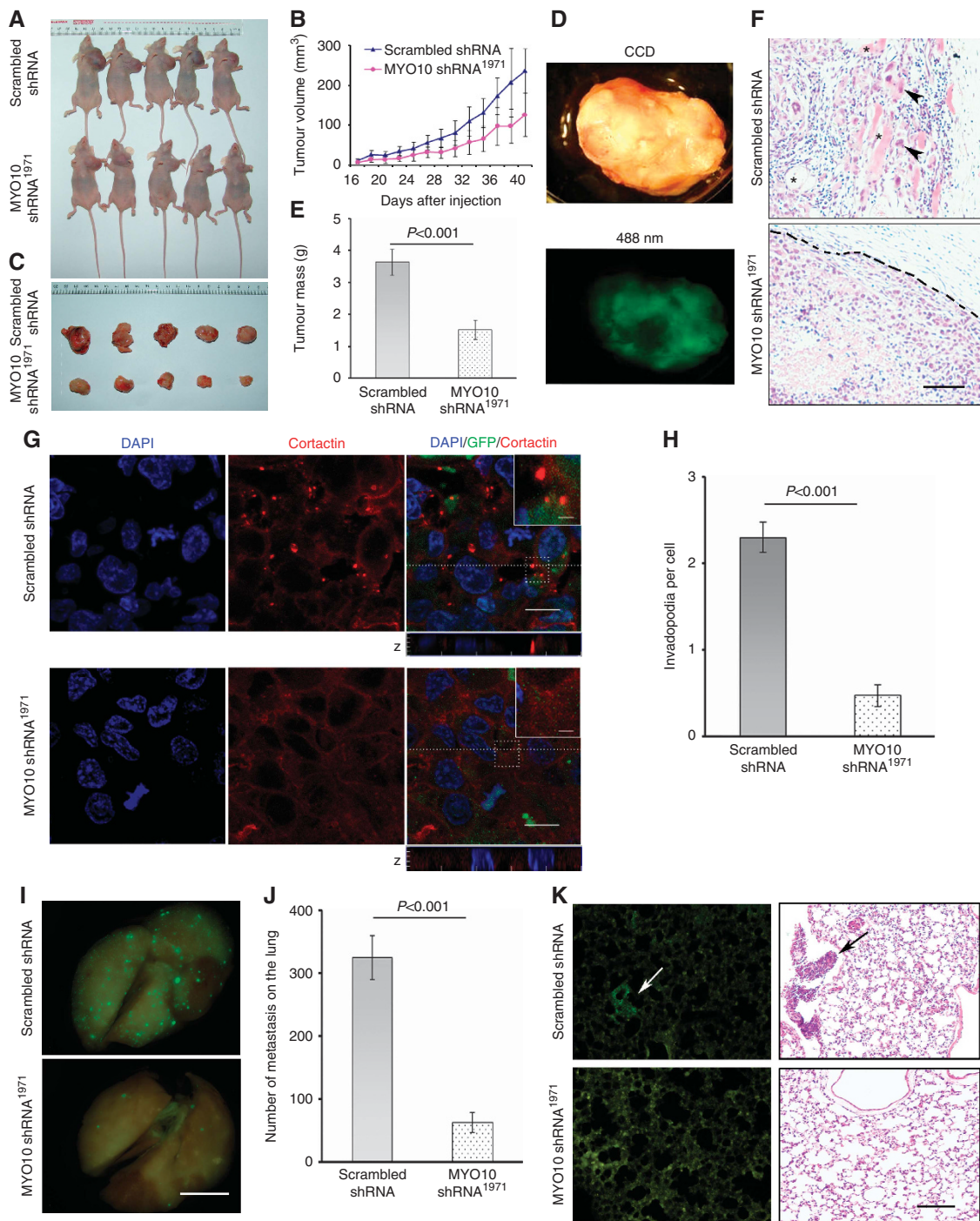


Figure 5. Silencing MYO10 inhibits tumour growth and lung metastasis in a nude mouse xenograft model. (A) Mice bearing tumours for 42 days. Cells expressing scrambled shRNA or MYO10 shRNA¹⁹⁷¹ were seeded into the left mammary fat pads of female BALB/c nude mice for 42 days. (B) Time course of tumour volumes in the scrambled shRNA and MYO10 shRNA¹⁹⁷¹ groups. (C) Tumours removed from mice. (D) A representative tumour tissue under visible light (upper panel) and under blue laser light (lower panel). (E) Tumour weight on day 42 post-inoculation (n = 5 per group, P = 0.003). (F) Representative images of paraffin tissue sections of primary tumours after HE staining. Tumour cells expressing scrambled shRNA invaded the surrounding stroma and adjacent adipose tissues (upper panel). Closed triangles indicate invasive tumour cells. Asterisks indicate adjacent adipose tissue. The tumour margin (including an intact capsule) in the MYO10 shRNA¹⁹⁷¹ tissue is indicated by a dashed line (lower panel). Bar, 100 μ m. (G) Images of primary tumour sections stained for cortactin (red), GFP (green), and DAPI (blue). A Z-section analysis revealed invadopodia, which were visible as cortactin-positive puncta, localised to the surface of the cells directly adjacent to the underlying matrix. Bars are 2.5 μ m for the insert and 10 μ m for the full images. (H) Quantification of the number of invadopodia per cell (n = 150 cells per sample). (I) Representative EGFP imaging revealing metastatic foci on the surface of lungs excised from mice expressing scrambled shRNA and MYO10 shRNA¹⁹⁷¹. Bar, 5 mm. (J) Quantification of EGFP-positive metastatic foci on the surface of the lung (n = 7 per group, P < 0.001). (K) Representative EGFP images demonstrating clustered cancer cells in frozen lung sections (left panel, arrow) and HE staining in paraffin-embedded tissue sections (right panel, arrow) from mice injected with scrambled shRNA- (upper panel) or MYO10 shRNA¹⁹⁷¹-transfected cells (lower panel). Bar, 80 μ m.

Furthermore, cells containing MYO10 shRNA¹⁹⁷¹ or scrambled shRNA were injected into the tail vein to investigate MYO10-dependent distant metastasis. The number of metastatic foci on the lung surface was significantly reduced in the MYO10 shRNA¹⁹⁷¹ group compared with the scrambled shRNA group (325 ± 93 per lung vs 54 ± 36 per lung, $P < 0.001$, Figure 5I and J). In addition, images of both the EGFP and HE sections revealed an obvious decrease in the number of clustered cancer cells in the lung when MYO10 was silenced (Figure 5K). These results in the animal xenograft model validated our findings in human breast cancer specimens that MYO10 was associated with tumour aggressiveness and metastasis.

DISCUSSION

Breast cancer patients with ER+ tumours are managed with a number of ER-targeted therapy options and/or chemotherapy; patients with Her2+ tumours receive Her2-directed therapy with trastuzumab or lapatinib. However, breast tumours lacking these markers (TNBC) are associated with more aggressive clinical behaviour and a poor prognosis (Reis-Filho and Tutt, 2008). Hence, finding new screening markers to distinguish TNBC from other subtypes is particularly important. Some proteins connected to filopodium formation or function have been reported to be related to cancer progression. Fascin, an actin-bundling protein involved in filopodial motility, is upregulated in several types of carcinomas; fascin upregulation is correlated with ER- breast cancer and a more aggressive clinical course (Arjonen *et al*, 2011). A recent study investigating the role of MYO10 in breast cancer revealed that MYO10, which is essential for filopodium formation, was required for breast cancer invasion by transporting integrins to filopodial tips (Arjonen *et al*, 2014). Here, we found that MYO10 was particularly elevated in TNBC tumours and promoted local invasion through invadopodia. The expression of *MYO10* was elevated in breast tumours and was correlated with ER- status, PR- status, and poor differentiation. Importantly, *MYO10* was associated with metastasis in TNBC patients, indicating the potential of MYO10 as a molecular marker to distinguish aggressive breast cancers.

The zinc finger transcription factor early growth response-1 (EGR1) has been demonstrated to have an important role in breast cancer migration, chemoinvasion, and xenograft growth (Mitchell *et al*, 2004). It has been reported that *MYO10* is a target gene of EGR1 in sarcoma cells with metastatic potential (Cermak *et al*, 2010). Interestingly, the hypothesis that MYO10 is upregulated by EGR1 was recently confirmed by a report that MYO10 was upregulated via an EGR1-dependent pathway in mutant p53 breast tumours (Arjonen *et al*, 2014). In accordance with that report, MYO10 was shown to be elevated in our study in BT-549 and MDA-MB-231 cells, both of which are p53 mutant. However, some patients with p53-positive tumours with metastatic potential (such as 50% of the TNBC patients) exhibited abundant *MYO10* expression, suggesting the existence of other potential activators of EGR1 in those patients. Mutant EGFR, for example, can also upregulate EGR1 expression (Maegawa *et al*, 2009).

Invadopodia are actin-rich structures believed to have a crucial role in cancer cell invasion through the degradation of the ECM. Although limited evidence suggests that MYO10 is one of the proteins involved in invadopodium formation (Schoumacher *et al*, 2010), our results identify MYO10 as a potential novel clinical marker for breast cancer based on correlations of elevated MYO10 expression with invadopodium formation and aggressive clinicopathological factors. MMP-14, MMP-9, and MMP-2 are the major proteases recruited by invadopodia to degrade the ECM (Muller *et al*, 2011). The localisation of MMP-14 to the invadopodia is a

key maturation step, which facilitates the secretion of active MMP-2 and MMP-9 by mature invadopodia to degrade the ECM (Weaver, 2006). Interestingly, we observed that silencing MYO10 led to MMP-14 downregulation and a reduction in the active MMP-9 in the extracellular milieu, suggesting that MYO10 promoted tumour invasion not only through its traditional role in invadopodia, as it does in filopodia, but also through the regulation of MMPs. This function is similar to that of cortactin, which is an actin assembly protein required for protease secretion in invadopodia-associated ECM degradation (Clark *et al*, 2007). MYO10, an actin-binding protein found in the leading edge of migrating cells, has no direct role in transcription. Silencing MYO10 downregulated several invadopodium-related genes, as shown by our microarray results. We hypothesise that silencing MYO10, which downregulated MMP-14 and reduced the active MMP-9, inhibited positive feedback from invadopodia, which led to the downregulation of those invadopodium-related genes.

Although MYO10 has previously been observed in invadopodia, how this protein participates in invasion and the biological function of its involvement in invadopodia remain unclear. MYO10 is considered a filopodium-related protein based on its role in transporting molecules such as integrins and VE-cadherin. We propose that MYO10 might also function as a transporter during invadopodium formation. Integrins are transmembrane adhesion proteins that link the cytoskeleton to the ECM and are presumed to mediate the adhesion of invadopodia to the ECM during invadopodial extension (Weaver, 2006). Moreover, integrins can serve as docking stations for ECM-degrading enzymes at invadopodia (Buccione *et al*, 2009). In this study, we determined that the activation of MYO10 in invadopodia was dependent on PtdIns(3,4,5)P₃, as in filopodia. We, thus, propose a working model of the function of MYO10 in invadopodia: MYO10 is auto-inhibited and transported to the plasma membrane by Rab7 vesicles, and clustered PtdIns(3,4,5)P₃ on the membrane recruits MYO10 by binding to MYO10's second PH domain. The activated MYO10 binds to β -integrins and transports them to the tips of invadopodia, where they can either mediate invadopodial adhesion to the ECM or dock MMPs to degrade the ECM during invasive growth or metastasis (Figure 6).

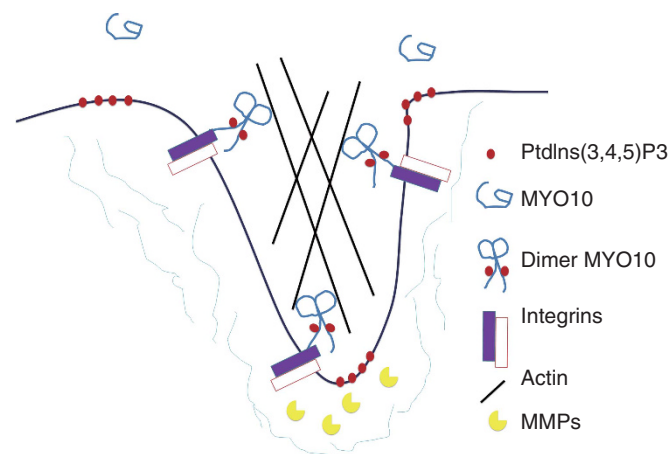


Figure 6. A working model of the function of MYO10 in invasive growth. In the cytoplasm, MYO10 is in an auto-inhibited and folded conformation. Clustered PtdIns(3,4,5)P₃ on the membrane recruits MYO10 by binding to its second PH domain; this opens the conformation and leads to the dimer formation of MYO10. The activated MYO10 binds to β -integrin and transports it to the tips of invadopodia, where it can either mediate the adherence of invadopodia to the ECM or dock MMPs, which degrade the ECM, and thereby promote invasive growth and metastasis.

In summary, this study systematically demonstrated an association between MYO10 and breast cancer aggressiveness and metastasis in clinical specimens and breast cancer cells. MYO10 was identified as a potential novel clinical marker for breast cancer based on the correlation between elevated MYO10 expression in tumours and invadopodium formation.

ACKNOWLEDGEMENTS

We thank Diter von Wettstein (Department of Crop and Soil Sciences, Washington State University, Pullman, WA, USA) and Wencheng Xiong (Georgia Health Sciences University, Augusta, GA, USA) for comments on the manuscript. Financial support was provided by the Program of Introducing Talents to Universities (B07017); the Project of National High Tech R&D Program (2009AA03Z308, 2011DFR51090); the Program for New Century Excellent Talents in University (NCET-07-0173); the National Natural Science Foundation of China (30871302, 301170142, 31271486); Jilin Provincial Research Foundation for Basic Research, China (200805130); the Fundamental Research Funds for the Central Universities (12SSXM005) and the Scientific Research Foundation from Northeast Normal University.

CONFLICT OF INTEREST

The authors declare no conflict of interest.

REFERENCES

- Akanuma N, Hoshino I, Akutsu Y, Murakami K, Isozaki Y, Maruyama T, Yusup G, Qin W, Toyozumi T, Takahashi M, Suito H, Hu X, Sekino N, Matsubara H (2014) MicroRNA-133a regulates the mRNAs of two invadopodia-related proteins, FSCN1 and MMP14, in esophageal cancer. *Br J Cancer* **110**: 189–198.
- Almagro S, Durmort C, Chervin-Petiot A, Heyraud S, Dubois M, Lambert O, Mailleraud C, Hewat E, Schaal JP, Huber P, Gulino-Debrac D (2010) The motor protein myosin-X transports VE-cadherin along filopodia to allow the formation of early endothelial cell-cell contacts. *Mol Cell Biol* **30**: 1703–1717.
- Arjonen A, Kaukonen R, Ivaska J (2011) Filopodia and adhesion in cancer cell motility. *Cell Adh Migr* **5**: 421–430.
- Arjonen A, Kaukonen R, Mattila E, Rouhi P, Hognas G, Sihto H, Miller BW, Morton JP, Bucher E, Taimen P, Virtakoivu R, Cao Y, Sansom OJ, Joensuu H, Ivaska J (2014) Mutant p53-associated myosin-X upregulation promotes breast cancer invasion and metastasis. *J Clin Invest* **124**: 1069–1082.
- Berg JS, Cheney RE (2002) Myosin-X is an unconventional myosin that undergoes intrafilopodial motility. *Nat Cell Biol* **4**: 246–250.
- Bloom HJ, Richardson WW (1957) Histological grading and prognosis in breast cancer; a study of 1409 cases of which 359 have been followed for 15 years. *Br J Cancer* **11**: 359–377.
- Buccione R, Caldieri G, Ayala I (2009) Invadopodia: specialized tumor cell structures for the focal degradation of the extracellular matrix. *Cancer Metast Rev* **28**: 137–149.
- Cermak V, Kosla J, Plachy J, Trejbalova K, Hejnar J, Dvorak M (2010) The transcription factor EGR1 regulates metastatic potential of v-src transformed sarcoma cells. *Cell Mol Life Sci* **67**: 3557–3568.
- Chen WT (1989) Proteolytic activity of specialized surface protrusions formed at rosette contact sites of transformed cells. *J Exp Zool* **251**: 167–185.
- Clark ES, Witham AS, Yarbrough WG, Weaver AM (2007) Cortactin is an essential regulator of matrix metalloproteinase secretion and extracellular matrix degradation in invadopodia. *Cancer Res* **67**: 4227–4235.
- Cortasio CL, Chan KT, Perrin BJ, Burton NO, Zhang S, Zhang ZY, Huttenlocher A (2008) Calpain 2 and PTP1B function in a novel pathway with Src to regulate invadopodia dynamics and breast cancer cell invasion. *J Cell Biol* **180**: 957–971.
- DeSantis C, Siegel R, Bandi P, Jemal A (2011) Breast cancer statistics. 2011. *CA Cancer J Clin* **61**: 409–418.
- Eckert MA, Lwin TM, Chang AT, Kim J, Danis E, Ohno-Machado L, Yang J (2011) Twist1-induced invadopodia formation promotes tumor metastasis. *Cancer Cell* **19**: 372–386.
- Fang Z, Yao W, Xiong Y, Zhang J, Liu L, Li J, Zhang C, Wan J (2010) Functional elucidation and methylation-mediated downregulation of ITGA5 gene in breast cancer cell line MDA-MB-468. *J Cell Biochem* **110**: 1130–1141.
- Gerhardt H, Golding M, Fruttiger M, Ruhrberg C, Lundkvist A, Abramsson A, Jeltsch M, Mitchell C, Alitalo K, Shima D, Betsholtz C (2003) VEGF guides angiogenic sprouting utilizing endothelial tip cell filopodia. *J Cell Biol* **161**: 1163–1177.
- Gianni L, Eiermann W, Semiglazov V, Manikhas A, Lluch A, Tjulandin S, Zambetti M, Vazquez F, Byakhov M, Lichinitser M, Climent MA, Ciruelos E, Ojeda B, Mansutti M, Bozhok A, Baronio R, Feyereislova A, Barton C, Valagussa P, Baselga J (2010) Neoadjuvant chemotherapy with trastuzumab followed by adjuvant trastuzumab versus neoadjuvant chemotherapy alone, in patients with HER2-positive locally advanced breast cancer (the NOAH trial): a randomised controlled superiority trial with a parallel HER2-negative cohort. *Lancet* **375**: 377–384.
- Gilles C, Bassuk JA, Pulyaeva H, Sage EH, Foidart JM, Thompson EW (1998) SPARC/osteonectin induces matrix metalloproteinase 2 activation in human breast cancer cell lines. *Cancer Res* **58**: 5529–5536.
- Giromoni M, Buccione R, Courtneidge SA, Linder S (2008) Assembly and biological role of podosomes and invadopodia. *Curr Opin Cell Biol* **20**: 235–241.
- Harper K, Arseneault D, Boulay-Jean S, Lauzier A, Lucien F, Dubois CM (2010) Autotaxin promotes cancer invasion via the lysophosphatidic acid receptor 4: participation of the cyclic AMP/EPAC/Rac1 signaling pathway in invadopodia formation. *Cancer Res* **70**: 4634–4643.
- Jordan VC, Morrow M (1999) Tamoxifen, raloxifene, and the prevention of breast cancer. *Endocr Rev* **20**: 253–278.
- Lv D, Zhang Y, Kim HJ, Zhang L, Ma X (2013) CCL5 as a potential immunotherapeutic target in triple-negative breast cancer. *Cell Mol Immunol* **4**: 303–310.
- Maegawa M, Arai Y, Yokote H, Matsumoto K, Kudo K, Tanaka K, Kaneda H, Fujita Y, Ito F, Nishio K (2009) EGFR mutation up-regulates EGR1 expression through the ERK pathway. *Anticancer Res* **29**: 1111–1117.
- Minn AJ, Gupta GP, Siegel PM, Bos PD, Shu W, Giri DD, Viale A, Olshen AB, Gerald WL, Massague J (2005) Genes that mediate breast cancer metastasis to lung. *Nature* **436**: 518–524.
- Mitchell A, Dass CR, Sun LQ, Khachigian LM (2004) Inhibition of human breast carcinoma proliferation, migration, chemoinvasion and solid tumour growth by DNazymes targeting the zinc finger transcription factor EGR-1. *Nucleic Acids Res* **32**: 3065–3069.
- Muller PA, Vousden KH, Norman JC (2011) p53 and its mutants in tumor cell migration and invasion. *J Cell Biol* **192**: 209–218.
- Park S, Koo JS, Kim MS, Park HS, Lee JS, Kim SI, Park BW (2012) Characteristics and outcomes according to molecular subtypes of breast cancer as classified by a panel of four biomarkers using immunohistochemistry. *Breast* **21**: 50–57.
- Plantard L, Arjonen A, Lock JG, Nurani G, Ivaska J, Stromblad S (2010) PtdIns(3,4,5)P(3) is a regulator of myosin-X localization and filopodia formation. *J Cell Sci* **123**: 3525–3534.
- Rakha EA, Reis-Filho JS, Baehner F, Dabbs DJ, Decker T, Eusebi V, Fox SB, Ichihara S, Jacquemier J, Lakhani SR, Palacios J, Richardson AL, Schnitt SJ, Schmitt FC, Tan PH, Tse GM, Badve S, Ellis IO (2010) Breast cancer prognostic classification in the molecular era: the role of histological grade. *Breast Cancer Res* **12**: 207.
- Reis-Filho JS, Tutt AN (2008) Triple negative tumours: a critical review. *Histopathology* **52**: 108–118.
- Schoumacher M, Goldman RD, Louvard D, Vignjevic DM (2010) Actin, microtubules, and vimentin intermediate filaments cooperate for elongation of invadopodia. *J Cell Biol* **189**: 541–556.
- Sousa AD, Cheney RE (2005) Myosin-X: a molecular motor at the cell's fingertips. *Trends Cell Biol* **15**: 533–539.
- Tokuo H, Ikebe M (2004) Myosin X transports Mena/VASP to the tip of filopodia. *Biochem Biophys Res Commun* **319**: 214–220.

- Weaver AM (2006) Invadopodia: specialized cell structures for cancer invasion. *Clin Exp Metast* **23**: 97–105.
- Wood W, Jacinto A, Grose R, Woolner S, Gale J, Wilson C, Martin P (2002) Wound healing recapitulates morphogenesis in *Drosophila* embryos. *Nat Cell Biol* **4**: 907–912.
- Workman P, Aboagye EO, Balkwill F, Balmain A, Bruder G, Chaplin DJ, Double JA, Everitt J, Farningham DA, Glennie MJ, Kelland LR, Robinson V, Stratford IJ, Tozer GM, Watson S, Wedge SR, Eccles SA. Committee of the National Cancer Research (2010) Guidelines for the welfare and use of animals in cancer research. *Br J Cancer* **102**: 1555–1577.
- Yamaguchi H, Condeelis J (2007) Regulation of the actin cytoskeleton in cancer cell migration and invasion. *Biochim Biophys Acta* **1773**: 642–652.
- Yamaguchi H, Takeo Y, Yoshida S, Kouchi Z, Nakamura Y, Fukami K (2009) Lipid rafts and caveolin-1 are required for invadopodia formation and extracellular matrix degradation by human breast cancer cells. *Cancer Res* **69**: 8594–8602.
- Yang X, Welch DR, Phillips KK, Weissman BE, Wei LL (1997) KAI1, a putative marker for metastatic potential in human breast cancer. *Cancer Lett* **119**: 149–155.
- Yu H, Wang N, Ju X, Yang Y, Sun D, Lai M, Cui L, Sheikh MA, Zhang J, Wang X, Zhu X (2012) PtdIns (3,4,5) P3 recruitment of Myo10 is essential for axon development. *PLoS One* **7**: e36988.
- Zhang H, Berg JS, Li Z, Wang Y, Lang P, Sousa AD, Bhaskar A, Cheney RE, Stromblad S (2004) Myosin-X provides a motor-based link between integrins and the cytoskeleton. *Nat Cell Biol* **6**: 523–531.
- Zhu XJ, Wang CZ, Dai PG, Xie Y, Song NN, Liu Y, Du QS, Mei L, Ding YQ, Xiong WC (2007) Myosin X regulates netrin receptors and functions in axonal path-finding. *Nat Cell Biol* **9**: 184–192.
- Zou KH, O'Malley AJ, Mauri L (2007) Receiver-operating characteristic analysis for evaluating diagnostic tests and predictive models. *Circulation* **115**: 654–657.

This work is published under the standard license to publish agreement. After 12 months the work will become freely available and the license terms will switch to a Creative Commons Attribution-NonCommercial-Share Alike 3.0 Unported License.

Supplementary Information accompanies this paper on British Journal of Cancer website (<http://www.nature.com/bjc>)